Novel Germanium-Based Magnetic Semiconductors

F. Tsui,[1,*] L. He,[1] L. Ma,[1] A. Tkachuk,[2] Y. S. Chu,[2] K. Nakajima,[3] and T. Chikyow[3]

[1]*Department of Physics and Astronomy, University of North Carolina, Chapel Hill, North Carolina 27599, USA*
[2]*Advanced Photon Source, Argonne National Laboratory, Argonne, Illinois 60439, USA*
[3]*National Institute for Material Science, Tsukuba, Ibaraki 305-0047, Japan*

(Received 12 June 2003; published 24 October 2003)

Epitaxial synthesis and properties of novel Co and Mn-doped Ge magnetic semiconductors were studied. Epitaxial growth of high quality films with high doping concentrations has been stabilized by the use of two dopants. The magnetic and transport properties of the system exhibit high T_C and large magnetoresistance effects that can be controlled systematically by the doping concentration. The maximum T_C achieved in the semiconducting materials is ~270 K at a composition of $Co_{0.12}Mn_{0.03}Ge_{0.85}$.

DOI: 10.1103/PhysRevLett.91.177203 PACS numbers: 75.50.Pp, 73.50.Jt, 75.70.–i

The prospect of integrating electron charge and spin degrees of freedom has invigorated the field of spin-polarized electronics, "spintronics" [1,2]. Most activities are focused on Mn-doped compounds of group III-V and II-VI families, where high quality ferromagnetic epitaxial films have been grown with Curie temperature T_C reaching 110 K [3]. However, there is considerable interest in higher T_C materials particularly in group IV elements, owing to their potential compatibility with current Si-based processing technology. Recent studies [4,5] show that Ge crystals doped with a transition metal element do exhibit ferromagnetism at low temperature but phase separation of dopant-rich compounds remains to be the main obstacle for achieving higher doping concentrations and producing higher T_C materials. Therefore, the bottleneck for implementing spintronics continues to be the lack of materials candidates. Here we report the synthesis and properties of high quality epitaxial films of high T_C magnetic semiconductors of Co and Mn-doped Ge. We show that doping with two elements can stabilize structures at higher doping concentrations than those doped with one of the elements, and that the strong interplay between structure and magnetism gives rise to novel magnetotransport phenomena.

Alloys of the form $Co_{ax}Mn_{bx}Ge_{1-x}$ were grown on undoped Ge (100) substrates using advanced combinatorial molecular beam epitaxy techniques [6]. Here a and b are the respective relative doping concentrations of Co and Mn with $a + b = 1$, and x is the total doping concentration. The experiments were designed to examine compositional dependence by employing a multilayer approach to vary x from 0 to 15 at. % on each substrate. Ge was doped at an interval of 2 Å alternately by depositing submonolayer wedges of Co and Mn using a precision mask, controlled by atomic absorption spectroscopy and quartz crystal monitors. Subsequent x-ray fluorescence spectroscopy (XFS) measurements confirmed the sample composition [7]. Electron-beam hearths were used to evaporate Ge and Co, an effusion cell was used for Mn, and a nominal deposition rate of ~0.1 Å/s was maintained. Pressure during synthesis was $\sim 10^{-10}$ torr. Preceding the film growth, each substrate was prepared through cycles of annealing-deposition-annealing, in order to produce an atomically smooth Ge (100) surface over the entire substrate. The doped films were grown at 250 °C and annealed at 450 °C, and were all about 1000 Å thick.

Structural properties were measured *in situ* by scanning reflection high-energy electron diffraction (RHEED), and *ex situ* by x-ray diffraction (XRD) [8] and high-resolution cross-sectional transmission electron microscopy (HRTEM). Magnetization was measured using SQUID magnetometry and, owing to the small sample size, the detection threshold was about $x =$ 3 at. %. In-plane electrical measurements were made using a four-terminal technique on samples that were cut to 2 mm by 0.5 mm. Transport parameters of the undoped substrate were measured and subtracted from the measurements.

Under the synthesis conditions outlined above, *in situ* RHEED measurements show that coherent two-dimensional (2D) epitaxial growth persists up to a doping concentration of x, above which the 2D features broaden and fade and epitaxial growth turns 3D, as illustrated in Figs. 1(a) and 1(b) by the RHEED intensity and width for a sample with $a/b \sim 2$. For larger x, the growth becomes increasingly disordered, as indicated by the decreasing diffraction intensity and rising diffused intensity. The doping concentration, at which the 2D to 3D transition occurs, exhibits a maximum around 15 at. % for Co-rich doping with a/b between 2 and 6, and minimum values of ~4 at. % at $a = 1$ (Co doping) and ~3 at. % at $b = 1$ (Mn doping). The films are stable at temperatures up to 600 °C during postgrowth annealing. Growth at temperatures below 200 °C is disordered.

Analyses of HRTEM [shown in Figs. 1(c) and 1(d)] and XRD experiments confirm that, below the 2D to 3D transition, the films exhibit a high degree of crystalline

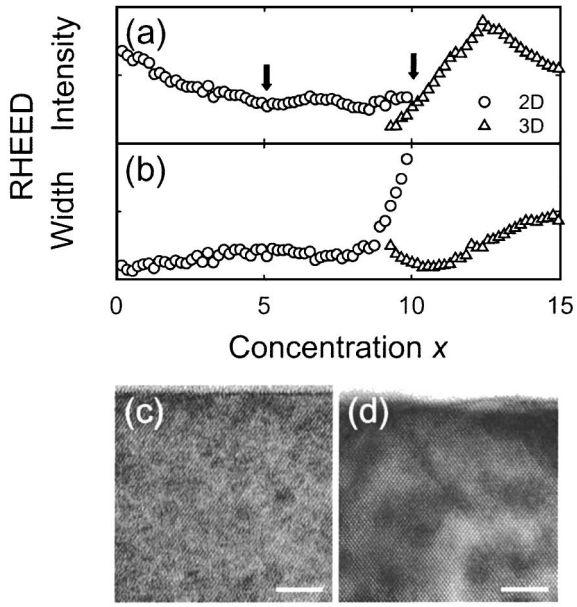

FIG. 1. Structure of $Co_{0.7x}Mn_{0.3x}Ge_{1-x}$ epitaxial films as a function of doping concentration x. Integrated RHEED intensity (a) and width (b) versus x. Circles are for the specular intensity and width of a 2D surface, and triangles are the corresponding zeroth order feature of a 3D surface. The arrows in (a) indicate the respective composition where the HRTEM images in (c) and (d) were taken. Each HRTEM image is 230 Å × 230 Å with the sample surface near the very top, and the scale bar in each image corresponds to 50 Å.

order without detectable impurity phases, evidently as a result of coherent pseudomorphic growth. The XRD results also show that, for Co-rich samples, below the transition the out-of-plane lattice is slightly compressed, $<0.1\%$, and near the transition the lattice relaxes. Since interstitial doping tends to expand the host lattice, the observed compressive strain indicates that the doping is mainly substitutional. In contrast, the observed relaxation may signal the onset of interstitial doping that gives rise to disorder and rough growth at higher x. The latter is consistent with the presence of dark regions in HRTEM images, as shown in Fig. 1(d).

Further analyses of XRD experiments reveal that the strain of the film exhibits distinct linear dependences with respect to Co and Mn concentrations. In particular, doping with Co in Ge contracts the lattice, while Mn doping expands it. The respective linear coefficients are -1.5×10^{-4} per Co at. % (compressive), and 4.5×10^{-4} per Mn at. % (tensile) [9], and they agree quantitatively with recent studies [10]. Our findings indicate that both kinetics and strain play key roles in stabilizing the smooth 2D epitaxial growth, and in inhibiting precipitation and growth of dopant-rich compounds; specifically, the presence of small lattice mismatch in Co-rich samples appears to stabilize alloy growth even at high doping levels. Details about the epitaxial growth and the structure will be reported elsewhere [11]. In what follows, we describe magnetic and transport effects and their interplay in the highly doped Co-rich materials with a/b ratios around 2.

$Co_{0.7x}Mn_{0.3x}Ge_{1-x}$ alloys order ferromagnetically with T_C and saturation magnetization M_s increasing with doping concentration, as shown in Fig. 2(a). T_C changes about 50% from $x \sim 2$ to 15 at. %, in qualitative agreement with a previous model prediction for Mn-doped Ge [4]. The M_s values correspond to an average moment per dopant ion of about $0.3\mu_B$, which is $\sim$10 times smaller than the known values for Co and Mn but comparable to those observed in some Mn-doped systems [12], indicating that only a fraction of dopants participate in the ordering. The field-cooled behavior under a field of 50 Oe differs from a Brillouin function, as shown in Fig. 2(b). The in-plane field-dependent hysteresis loops exhibit relatively small remanence, and a small saturation field of a few hundred Oe, as shown in Fig. 2(c). Like its structural counterparts, the magnetism also depends sensitively on doping concentration and synthesis conditions. The highest T_C achieved thus far for semiconductors is $\sim$270 K at $a/b \sim 4$ and $x \sim 15$ at. %.

Temperature-dependent transport parameters for various doping concentrations are shown in Fig. 3. Below the Ge intrinsic regime [indicated by the solid lines in Figs. 3(a) and 3(b)], resistivity ρ_{xx} exhibits a peak around 180 K, a valley around 60 K, and two exponential regions with respect to $1/T$ at low temperatures [the dashed lines in Fig. 3(a)]. The ordinary Hall coefficient R_0, on the other hand, first changes sign near 320 K from negative to positive, signaling the onset of p-type extrinsic transport, and it exhibits two unusual sign changes at low temperatures, from positive to negative [arrows in Fig. 3(b)] and back to positive. Correspondingly, the

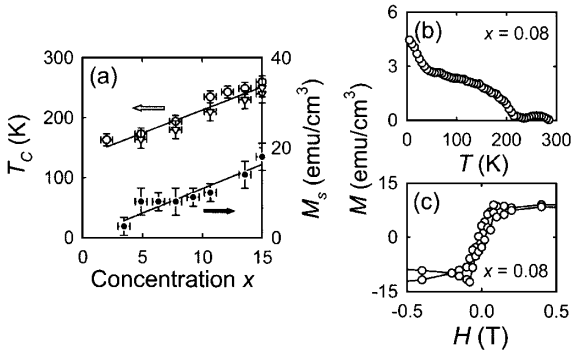

FIG. 2. Magnetism of $Co_{0.7x}Mn_{0.3x}Ge_{1-x}$ epitaxial films as a function of doping concentration x. (a) T_C (open symbols) and M_s (closed circles) versus x. The T_C values were determined by SQUID magnetometry (triangles) and by an Arrott plot of the magnetotransport parameters (circles). The latter is discussed in the text associated with Fig. 5. The lines are to guide the eyes. Large uncertainties are due to small sample size. (b) Field-cooled magnetization under 50 Oe, and (c) hysteresis loop at 5 K for a sample with $x \sim 8$ at. %.

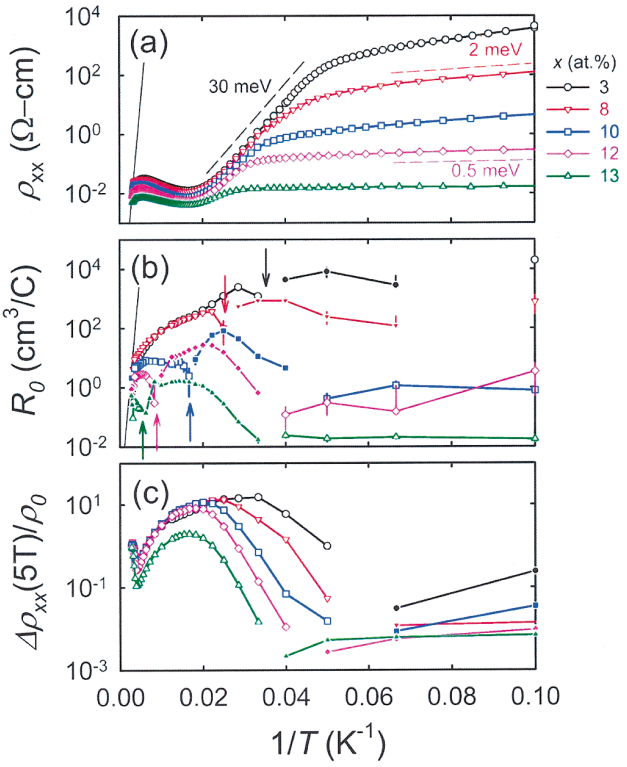

FIG. 3 (color online). Magnetotransport parameters of $Co_{0.7x}Mn_{0.3x}Ge_{1-x}$ versus $1/T$ at various x. (a) Zero-field resistivity ρ_{xx} (also defined as ρ_0). The solid line corresponds to the intrinsic regime with activation energy of 0.33 eV, and dashed lines indicate various low temperature activation energies. (b) Ordinary Hall coefficient R_0. The solid line also corresponds to the intrinsic regime, and arrows indicate the first sign change from positive to negative at T_H. (c) MR ratio $\Delta\rho_{xx}/\rho_0$ at $H = 5$ T, where $\Delta\rho_{xx} = \rho_{xx}(H = 5\text{ T}) - \rho_0$. In both (b) and (c), open and closed symbols indicate positive and negative values, respectively.

magnetoresistance (MR) ratio [Fig. 3(c)] exhibits a minimum around 240 K and, as the temperature decreases, it first rises to a large peak (> 10 for $x < 10$ at. %) at T_{MR}, and then falls sharply and eventually changes sign at low temperature.

The presence of a maximum in ρ_{xx} indicates that the transport in this temperature range is strongly influenced by scattering effects but, since the peak temperature does not scale with T_C, the effect of magnetic critical scattering is relatively weak. At low temperatures, the exponential regime with activation energy of ~30 meV [Fig. 3(a)], nearly common to all doping levels, is most likely to be associated with a shallow acceptor level, but the counterpart at lower activation energy together with the sign changes of R_0 indicates the presence of significant impurity band conduction. For $x < 10$ at. %, ρ_{xx} exhibits the Mott $T^{-1/4}$ law down to 1.7 K, indicating that the variable range hopping is the dominant mechanism for transport in the impurity band, and therefore the first sign change of R_0 from positive to negative at T_H [arrows in Fig. 3(b)] can be viewed as the onset of the hopping dominated regime.

The sharp fall of the MR ratio [Fig. 3(c)] correlates with the sign change of R_0 at T_H [Fig. 3(b)]. This reveals that the large positive MR effect is associated with the hole conduction. Furthermore, as shown in Fig. 4, both T_{MR} and T_H correlate with T_C, particularly for $x <$ 10 at. %. These findings indicate that the doping concentration controls both the magnetism and low temperature transport phenomena.

The observed temperature dependence exhibits the characteristics of a highly doped Ge with a shallow acceptor level [13], which is surprisingly low when compared to the known values for Co and Mn (>160 meV above the valence band) [14]. Co also has a donor level in Ge about 90 meV above the valence band that can give rise to compensation effects. In fact, carrier concentration estimated from R_0 at room temperature varies from 5×10^{17} cm^{-3} to 5×10^{19} cm^{-3}; that is about 1000 times smaller than the respective doping concentrations, indicating that the alloys are indeed highly compensated. Random distribution of the Co donor impurities also represents a fluctuating potential that can cause broadening of the impurity band [15], in addition to the broadening and perhaps splitting caused by the presence of high doping level and exchange interactions. While these effects may give a reasonable explanation to the apparent shallow acceptor level of 30 meV, additional experiments that probe the impurity band directly are necessary in order to elucidate this.

Hall mobility (R_0/ρ_{xx}) has been estimated from the measurements shown in Fig. 3. At room temperature, it ranges from 10^3 to 10^2 cm^2/V s with respect to x from 1 to 15 at. %, and as temperature decreases it rises to a peak well above 10^4 cm^2/V s for $x < 10$ at. % around T_{MR}, before falling more than a factor of 100 at low temperatures. The observed high values at low doping

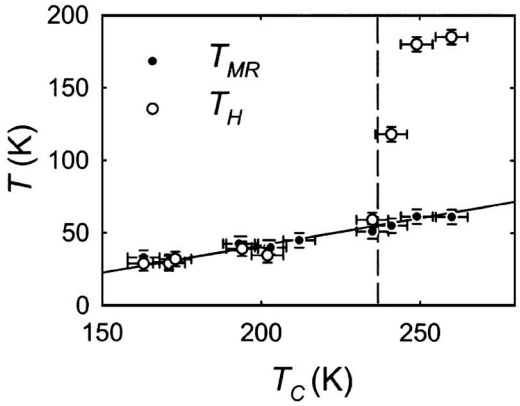

FIG. 4. Correlation between transition temperatures: T_{MR} (closed circles) and T_H (open circles) versus T_C. The vertical line separates doping concentration x above (right) and below (left) 10 at. %.

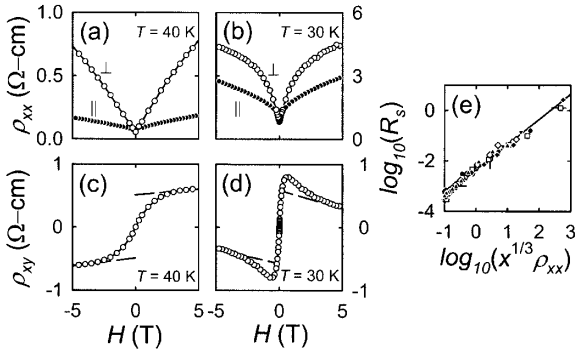

FIG. 5. (a)–(d) Characteristic field-dependent transport effects below T_C for $Co_{0.7x}Mn_{0.3x}Ge_{1-x}$ at $x \sim 8$ at. %. Open circles indicate data for fields applied perpendicular to the film ($\perp$), and closed circles indicate those for fields applied along the current direction ($\parallel$). The dashed lines in (c) and (d) indicate the linear behavior at high field, from which both R_0 and R_s are determined. (e) The linear scaling of R_s and ρ_{xx} at 5 T for $x < 10$ at. % at temperatures between T_C and T_H. The factor $\sqrt[3]{x}$ corresponds to a nominal linear spacing between dopants. The line is a linear fit of the data, and the different symbols correspond to nine different samples with different x.

levels are comparable to those observed in high purity Ge, indicating the presence of the long carrier mean-free path that is consistent with the high structural quality of the material. In contrast, the low temperature counterparts confirm the presence of impurity band conduction.

The field-dependent behaviors of ρ_{xx} and Hall resistivity ρ_{xy} are illustrated in Fig. 5. Below the intrinsic regime, ρ_{xx} at low fields changes from quadratic to linear behavior [Fig. 5(a)], while ρ_{xy} becomes nonlinear owing to the presence of magnetization-dependent extraordinary Hall effect (EHE) [Fig. 5(c)]. The latter follows the phenomenological form of $R_0H + R_s 4\pi M$ [16], where the first term is the ordinary Hall effect and the second is the EHE with respective coefficients R_0 and R_s.

The ratio of ρ_{xy}/ρ_{xx} scales with M quite well over a wide range of temperature around T_C, such that quantitative values of T_C [the circles in Fig. 2(a)] can be obtained by using an Arrott plot of $(\rho_{xy}/\rho_{xx})^2$ versus $H/(\rho_{xy}/\rho_{xx})$ (Ref. [3]), analogous to that for a ferromagnetic equation of state. As the temperature decreases, the low-field slope of ρ_{xx} increases [Fig. 5(b)], while the high-field slope of ρ_{xy} (i.e., R_0) decreases and changes sign at T_H [Fig. 5(d)], as discussed above. ρ_{xy} becomes more nonlinear, while exhibiting a peak. The ρ_{xy}/ρ_{xx} ratio no longer scales with M, and it also exhibits an unusually large peak (>1) at low field, which most likely arises from a substantially different spin-dependent carrier lifetime between the holes in the valence band and the electrons in the impurity band [16]. In other words, the two types of carriers exhibit drastically different field-dependent responses. This interpretation is also consistent with the observed low temperature sign change of MR and the associated nonmonotonic field dependence.

At temperatures above the hopping regime, R_s and ρ_{xx} at 5 T correlate linearly with each other, as shown in Fig. 5(e). The correlation indicates that the carrier relaxation is very weak leading to plane wave states and thus giving rise to the classical skew scattering. This observation, when combined with features such as shallow impurity level, large MR effects, high T_C, and compatibility with Si, makes the material quite desirable for exploring spintronics. The viability of the system has been further demonstrated by the recent observation of a large magnetization-dependent rectification effect in heterojunction diodes made from these materials [17].

In summary, synthesis and properties of a new class of Ge-based magnetic semiconductors have been studied. High quality epitaxial films with high doping concentrations can be grown on Ge (100) by using two dopants, Co and Mn, in order to stabilize the epitaxial growth. The approach opens avenues for synthesizing a wide range of electronic materials. The magnetic and transport properties of the system exhibit novel behavior that can be controlled systematically by the doping concentration.

We thank Stefan Vogt at APS for experimental assistance. The work was supported in part by NSF DMR-0108605. Use of the Advanced Photon Source was supported by the U.S. Department of Energy, Basic Energy Sciences, Office of Science, under Contract No. W-31-109-Eng-38.

*Author to whom correspondence should be addressed. Electronic address: ftsui@physics.unc.edu

[1] G. A. Prinz, Phys. Today **48**, 58 (1995).
[2] S. Das Sarma, Am. Sci. **89**, 516 (2001).
[3] H. Ohno, Science **281**, 951 (1998).
[4] Y. D. Park *et al.*, Science **295**, 651 (2002).
[5] S. Choi *et al.*, Appl. Phys. Lett. **81**, 3606 (2002).
[6] Y. K. Yoo and F. Tsui, MRS Bull. **27**, 316 (2002).
[7] S. Vogt *et al.*, Appl. Surf. Sci.(to be published).
[8] XFS and XRD measurements were carried out at beam line 2-BM of the Advanced Photon Source.
[9] There is an uncertainty of ~25% from estimates of doping concentrations.
[10] R. K. Iwanowski, K. Lawniczak-Jablonska, Z. Golacki, and A. Traverse, Chem. Phys. Lett. **283**, 313 (1998).
[11] F. Tsui, L. He, A. Tkachuk, S. Vogt, and Y. S. Chu (unpublished).
[12] H. Ohldag *et al.*, Appl. Phys. Lett. **76**, 2928 (2000).
[13] H. Fritzsche, Phys. Rev. **99**, 406 (1955).
[14] H. H. Woodbury and W. W. Tyler, Phys. Rev. **100**, 659 (1955).
[15] O. Madelung, *Introduction to Solid State Theory* (Springer-Verlag, Berlin, 1981), Chap. 10.
[16] C. M. Hurd, *The Hall Effect in Metals and Alloys* (Plenum, New York, 1972).
[17] F. Tsui, L. Ma, and L. He, Appl. Phys. Lett. **83**, 954 (2003).